Scaling of the Quantum Anomalous Hall Effect as an Indicator of Axion Electrodynamics

S. Grauer, K. M. Fijalkowski, S. Schreyeck, M. Winnerlein, K. Brunner, R. Thomale, C. Gould, and L. W. Molenkamp
Faculty for Physics and Astronomy (EP3 and TP1), Universität Würzburg, Am Hubland, D-97074 Würzburg, Germany
(Received 26 October 2016; revised manuscript received 16 May 2017; published 16 June 2017)

We report on the scaling behavior of V-doped $(\mathrm{Bi},\mathrm{Sb})_2\mathrm{Te}_3$ samples in the quantum anomalous Hall regime for samples of various thickness. While previous quantum anomalous Hall measurements showed the same scaling as expected from a two-dimensional integer quantum Hall state, we observe a dimensional crossover to three spatial dimensions as a function of layer thickness. In the limit of a sufficiently thick layer, we find scaling behavior matching the flow diagram of two parallel conducting topological surface states of a three-dimensional topological insulator each featuring a fractional shift of $\frac{1}{2}e^2/h$ in the flow diagram Hall conductivity, while we recover the expected integer quantum Hall behavior for thinner layers. This constitutes the observation of a distinct type of quantum anomalous Hall effect, resulting from $\frac{1}{2}e^2/h$ Hall conductance quantization of three-dimensional topological insulator surface states, in an experiment which does not require decomposition of the signal to separate the contribution of two surfaces. This provides a possible experimental link between quantum Hall physics and axion electrodynamics.

DOI: 10.1103/PhysRevLett.118.246801

Introduction.—After several theoretical proposals to accomplish the quantum anomalous Hall effect (QAHE) [1–5], it has recently been observed in magnetically doped $(\mathrm{Bi},\mathrm{Sb})_2\mathrm{Te}_3$ [6–14]. The exact quantization and edge channel transport have been verified. Theory has suggested the system may be a suitable host for the realization of Majorana bound states [15] by combining superconductivity with the QAHE, and exploring quantized signatures of the three-dimensional topological magnetoelectric effect [5,16,17].

The QAHE has thus far been observed in thin layers with thicknesses in the range of 4 to 10 nm which are typically described as thin films. The onset of a gap stemming from the hybridization of the top and bottom surface state is predicted to be in the range of 6 nm [18,19], which is also the thickness at which opening of the gap was observed in ARPES measurements on Bi_2Se_3 by Zhang *et al.* [20], and also in layers grown by our group [21]. While many of the QAHE layers reported on so far are thinner than 6 nm, some are not. Also, layer roughness, resulting in part from the existence of rotation twins [22], makes it difficult to define an exact layer thickness. It is therefore not clear if the layers should be regarded as magnetic 2D or 3D topological insulators (TIs).

The mechanism invoked to explain the QAHE in its initial manifestation [6] is applicable to a 2D system [3], where the inversion of one spin species is lifted by exchange interaction. The theoretical perspective on the QAHE at a 3D TI surface, however, is different, and is tied to the axion term [23] characterizing the electrodynamic response of a 3D TI bulk [24]. This has recently been investigated through Faraday and Kerr rotation spectroscopy [25–27], where one observes the joint effect of both topologically nontrivial surfaces and has no measure to decompose the signal into individual surface contributions. Because of the effect of the axionic action $S_\theta = (\theta\alpha/4\pi)\int \boldsymbol{E}\cdot\boldsymbol{B}d^3xdt$, where α is the fine structure constant and $\theta = 1$ in the TI bulk up to its boundary, the single Dirac cone surface state does not violate gauge symmetry upon minimal coupling to an electromagnetic field [28,29]. As the magnetic dopants induce a gap and magnetic disorder might act to further localize the Dirac surface density of states, a half-integer contribution to the Hall conductivity $\sigma_{xy} = \pm\frac{1}{2}e^2/h$ is still expected to be observable as long as the Fermi level resides in the 3D TI bulk gap [5]. The surface state of a 3D TI exhibiting the QAHE could thus be regarded as an "axion insulator".

In this Letter, we report on our measurements on $\mathrm{V}_y(\mathrm{Bi}_{1-x}\mathrm{Sb}_x)_{2-y}\mathrm{Te}_3$ layers with thicknesses around 9 nm which match the predicted flow diagram of two parallel topological surface states, providing an experimental signature of a QAHE quantized in units of $\sigma_{xy} = \pm\frac{1}{2}e^2/h$ on each of the two surfaces, e.g., the top and bottom, of a magnetic 3D TI slab. This effect is best evidenced by examining flow diagrams describing the relation of the longitudinal σ_{xx} to the transversal σ_{xy} conductivities during the transition from one filling factor to another. A flow diagram of the QAHE was first reported by Checkelsky *et al.* [7] and resembles that of the integer quantum Hall effect (IQHE) [30] where the relation between σ_{xx} and σ_{xy} follows semicircles centered on $(\sigma_{xy},\sigma_{xx}) = (\frac{1}{2}e^2/h, 0)$ and $(-\frac{1}{2}e^2/h, 0)$, going through the points $(e^2/h, 0)$, (0,0), and $(-e^2/h, 0)$. Both components of the conductance going to zero during the transition indicate a complete breakdown of the edge channel transport. By extracting the values of σ_{xx} and σ_{xy} from published measurements of the external magnetic field dependence to

determine their scaling diagram, one finds that most subsequent observations of the QAHE show the same behavior. This can be directly seen by the peak value of the longitudinal resistivity $\rho_{xx} > h/e^2$ at $\rho_{xy} = 0$. Examples of such a high longitudinal resistivity are measurements with $\rho_{xx} = 2.2h/e^2$ in Fig. 2 of Ref. [6], $\rho_{xx} = 2.1h/e^2$ in Fig. 2 of Ref. [7], $\rho_{xx} = 1.7h/e^2$ in Fig. 1 of Ref. [10], $\rho_{xx} = 1.6h/e^2$ in Fig. 4 of Ref. [11], or even as high as $\rho_{xx} = 34h/e^2$ in Fig. 1 of Ref. [12]. The lowest peak values of the longitudinal resistivity are seen in Fig. 1 of Ref. [9] with $\rho_{xx} = 1.1h/e^2$ which, with a thickness of 10 nm, is measured on the thickest layer of the listed experiments. While our control measurements on thin layers show this same scaling behavior, our slightly thicker samples show the transition to the very different scaling behavior consistent with that predicted for an axion insulator.

Magnetic 3D TI layers.—Our $V_y(Bi_{1-x}Sb_x)_{2-y}Te_3$ layers are grown by molecular beam epitaxy on Si(111) and InP(111) substrates and capped *in situ* with a 10 nm layer of Te as protection against the environment. The V content y was determined from the growth rate of pure V to be $y \approx 0.1$ for all layers, the varying Sb content x is determined by x-ray diffraction (XRD) measurements of the lateral lattice constant a and the layer thicknesses are obtained from x-ray reflection (XRR) measurements [31]. After growth, the layers are patterned into Hall bar devices with a top gate and AuGe contacts using standard optical lithography (see Supplemental Material [32] for more details). All presented transport measurements were conducted at base (nominally 25 mK) temperature (unless specified otherwise) in a dilution refrigerator equipped with a high field magnet. Hall and longitudinal resistances were measured using standard high-precision, low-frequency ac techniques (2–14 Hz). In all cases, the dependence of the longitudinal (ρ_{xx}) and Hall resistivity (ρ_{xy}) on the gate voltage was first measured in the absence of a magnetic field, and all magnetoresistivity data presented in the Letter are then taken for the gate voltage condition which gives the maximum value of ρ_{xy} (unless specified otherwise).

Figure 1 shows a measurement of the longitudinal and Hall resistivity of several samples in an external magnetic field: Five 9-nm-thick layers with varying composition $V_{0.1}(Bi_{1-x}Sb_x)_{1.9}Te_3$, an 8-nm-thick $V_{0.1}(Bi_{0.22}Sb_{0.78})_{1.9}Te_3$ layer, and a 6-nm-thick $V_{0.1}(Bi_{0.21}Sb_{0.79})_{1.9}Te_3$ layer. The ρ_{xy} data of Fig. 1(a) shows that all layers are in the QAH regime and at least close to quantization, with $\rho_{xy}(H = 0) > 0.8h/e^2$. The longitudinal resistivity shown in Fig. 1(b), on the other hand, shows results that can be classified into two distinct categories. For all layers with $d \approx 9$ nm, the peak value of ρ_{xx} is less than h/e^2, while the layers with $d < 9$ nm, in contrast, show a peak value which is higher than h/e^2, as is common in the literature.

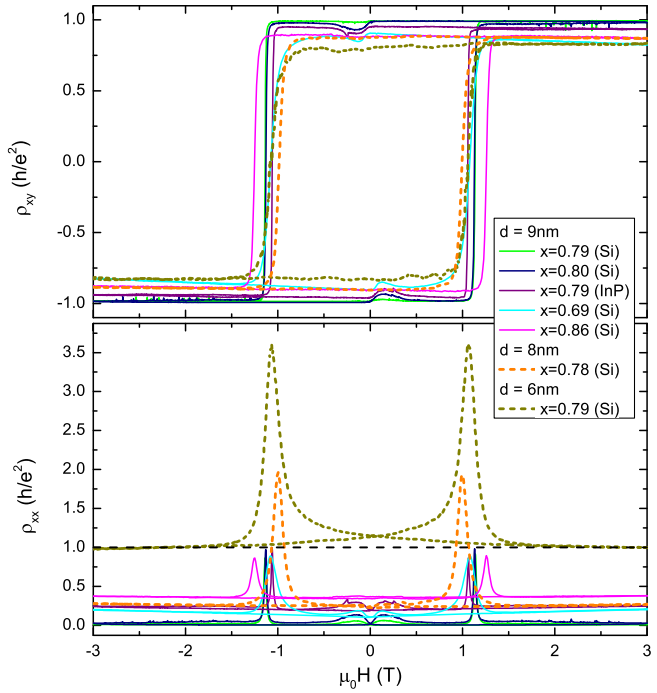

FIG. 1. ρ_{xy} (a) and ρ_{xx} (b) of several $V_{0.1}(Bi_{1-x}Sb_x)_{1.9}Te_3$ layers as a function of the external magnetic field. The varied parameters are the Sb content x, the layer thickness d, and substrate type. The data acquired on the five layers with $d \approx 9$ nm are displayed as solid lines. Four of them are grown on Si(111) with x values of 0.69 (cyan), 0.79 (green), 0.80 (navy), 0.86 (magenta). One is grown on InP(111) with $x = 0.79$ (purple). The measurements of two thinner layers with $d = 8$ nm and $x = 0.78$ (orange) and $d = 6$ nm and $x = 0.79$ (dark yellow), grown on Si (111), are displayed as dashed lines.

Flow diagrams of these measurements for the $d \approx 9$ nm layers are shown in Fig. 2. These diagrams show the scaling of σ_{xx} to σ_{xy} as an external parameter is used to turn the system between plateaus. Any external parameter which affects the plateau transition can be used. In this Letter we choose to use external magnetic field as a parameter [30,33,34] as it allows us to access a larger area of phase space while at the same time protecting the insulation nature of the bulk. Scaling diagrams using parameters such as temperature and gate voltage are shown in the Supplemental Material [32]. The transition does not occur via the insulating state at (0,0), but rather different behavior is observed. Instead of following the above described flow diagram of the IQHE (black dashed lines), the data follow a semicircle centered on the origin with a radius of e^2/h (red dashed line).

Such a semicircle centered on the origin is exactly what is predicted for a topological surface state in a magnetic 3D TI. Nomura and Nagaosa studied the transition of half-integer quantized states from $\sigma_{xy} = \frac{1}{2}e^2/h$ to $\sigma_{xy} = -\frac{1}{2}e^2/h$ on a single surface of a TI [5], and found a scaling behavior shown by the green dashed line in Fig. 2, a semicircle which connects the two points $(\frac{1}{2}e^2/h,0)$ and

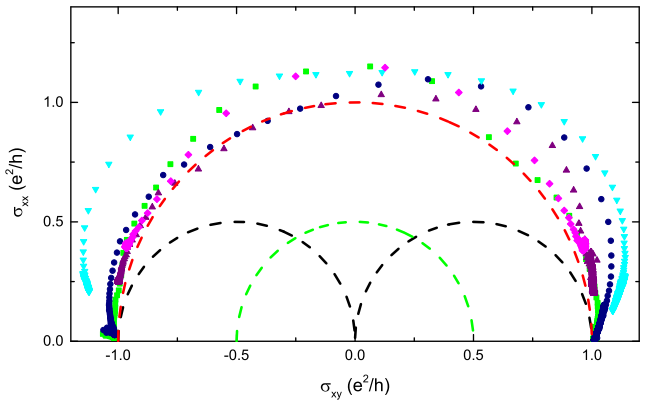

FIG. 2. Flow diagram mapping σ_{xx} to σ_{xy} of layers with $d \approx 9$ nm from the external magnetic field measurement (see Fig. 1) is shown. The black dashed line represents the flow diagram of the IQHE, the green dashed line the predicted flow diagram of a single topological surface state, and the red dashed line two parallel conducting topological surface states. The color code of the measurement data is the same as in Fig. 1.

$(-\frac{1}{2}e^2/h,0)$ without transitioning through the insulating state. For two parallel conducting surface states, e.g., the top and bottom surface of the layer, the conductivities add and the resulting scaling behavior is represented by the red dashed line in Fig. 2, consistent with our observed behavior. It is worth noting that the key distinction between the IQHE and the axionic behavior is the position of the center of the semicircle in the flow diagram, which is at $\sigma_{xy} = \frac{1}{2}e^2/h$ for the former case, and shifted back by $\frac{1}{2}e^2/h$ in the latter. This shift from finite value to zero does not depend on the number of surfaces being considered and thus is robust evidence of a fundamentally different scaling, which is consistent with an axionic term acting on a single topological surface state.

Robustness of the effect.—To further confirm the robustness of the axionic scaling, we present flow diagram analysis for our representative perfectly quantized 9-nm-thick $V_{0.1}(Bi_{0.21}Sb_{0.79})_{1.9}Te_3$ layer [14], for a wide range of fixed gate voltage values in Fig. 3, and for various fixed temperature values in Fig. 4. As expected, so long as the Fermi level resides in the bulk band gap, change in carrier concentration does not affect the scaling properties of such a system. Similar reproducible behavior characterizes the magnetic field scans at elevated temperatures, as clearly seen in Fig. 4. Magnetoresistivity measurements at temperatures ranging from base temperature of the dilution refrigerator up to 1 K, reveal nearly constant longitudinal resistivity peak values, while high field values increase from 0 to nearly $0.5h/e^2$, as seen in the Supplemental Material, Fig. 4 [32]. The same conclusion applies to magnetoresistivity scans for different gate voltage values visible in the Supplemental Material, Fig. 3 [32], where the ρ_{xx} peak value again proves to be nearly carrier concentration independent and close to the quantized value h/e^2.

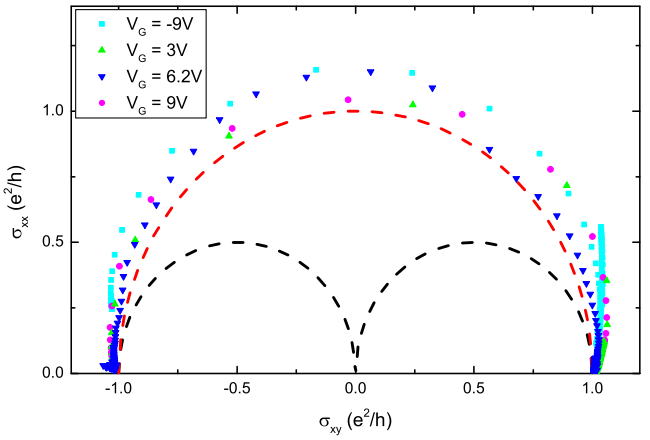

FIG. 3. Flow diagram mapping σ_{xx} to σ_{xy} for four different fixed gate voltage values $V_G = -9$ V (cyan), $V_G = 3$ V (green), $V_G = 6.2$ V (blue), and $V_G = 9$ V (magenta), for a representative 9-nm-thick $V_{0.1}(Bi_{0.21}Sb_{0.79})_{1.9}Te_3$ layer exhibiting perfectly quantized transport (green in Fig. 1, Fig. 2, and Fig. 5). The black dashed line represents the flow diagram of the IQHE and the red dashed line two parallel conducting topological surface states.

Sensitivity to layer thickness.—We first note that because $(Bi, Sb)_2Te_3$ grows with rotational twins, no perfectly flat layer in this material system has ever been achieved, and the typical surface roughness is not negligible compared to layer thicknesses. As such, layer thicknesses reported by various groups using methodologies, which are effected differently by this roughness, are difficult to compare. The values of the layer thicknesses given here should therefore be viewed as a way to reliably compare the relative thicknesses of our samples, but will not necessarily compare in absolute values to those reported by other groups. Having said that, to

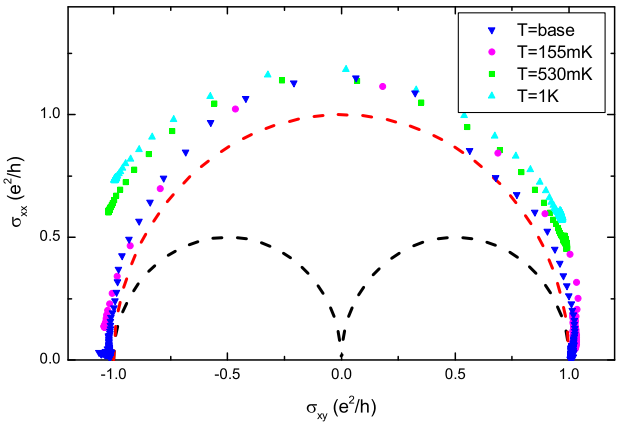

FIG. 4. Flow diagram mapping σ_{xx} to σ_{xy} for four different fixed temperature values $T = 155$ mK (magenta), $T = 530$ mK (green), $T = 1$ K (cyan), and base temperature of the dilution refrigerator (blue) for a representative 9-nm-thick $V_{0.1}(Bi_{0.21}Sb_{0.79})_{1.9}Te_3$ layer exhibiting perfectly quantized transport (green in Fig. 1, Fig. 2, and Fig. 5). The black dashed line represents the flow diagram of the IQHE and the red dashed line two parallel conducting topological surface states.

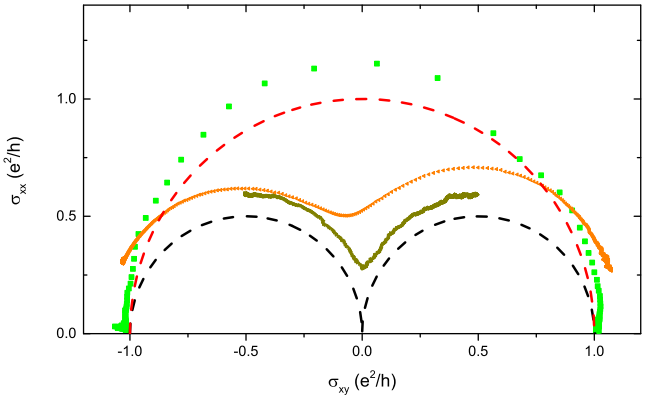

FIG. 5. Flow diagram mapping σ_{xx} to σ_{xy} for three different layers with $d = 9$ nm (green), $d = 8$ nm (orange), and $d = 6$ nm (dark yellow) and similar composition, as extracted from the external magnetic field measurement (see Fig. 1). The black dashed line represents the flow diagram of the IQHE and the red dashed line two parallel conducting topological surface states.

confirm that thickness is indeed the key parameter distinguishing between the IQHE and axionic scaling, we reproduce the scaling curve of a 9-nm-thick layer exhibiting perfectly quantized transport, together with that of an 8-nm and a 6-nm-thick layer of similar composition in Fig. 5. Already for the 8-nm-thick layer, a clear deviation from the 3D TI axionic scaling behavior is seen in the form of a dip at $\sigma_{xy} = 0$. This feature strengthens for the 6-nm-thick layer, which qualitatively follows the IQHE flow diagram represented by the black dashed line. Although both the 8 nm and 6 nm layers do not accurately quantize, they are in the QAHE regime and show a transition in scaling behavior, from the axionlike scaling expected in the 3D case to the previously reported IQHE scaling, highlighting the existence of two distinct regimes of QAHE. Unfortunately layers of even greater thickness cannot be studied as bulk contributions begin to significantly influence the observed transport as shown in the Supplemental Material, Fig. 2 [32].

Finally, we remark on the significance of the protective Te cap. Samples which are grown without a cap and otherwise processed in the same way, also exhibit the QAHE effect. The flow diagrams extracted from the external magnetic field dependence of three uncapped layers are shown in the Supplemental Material, Fig. 6 [32]. All three of these layers are at least 9 nm thick as determined by XRR measurements, yet show 2D scaling behavior. The flow diagram of uncapped layers therefore matches the scaling behavior of thinner capped layers. This is likely to be a result of degradation in the topmost layers due to exposure of the unprotected surface to ambient conditions and the lithography process, and suggests that uncapped samples have a dead layer at their surface, and thus are effectively thinner than their nominal values.

The range of thickness at which we see the scaling transition in capped layers is not inconsistent with the expected opening of the hybridization gap at 6 nm. While most of the samples reported on in the literature are below this threshold, a clear IQHE scaling behavior is also seen in measurements from Checkelsky *et al.* [7] and Bestwick *et al.* [9] on layers which are nominally 8 nm and 10 nm thick, respectively. Considering that magnetically doped $(Bi, Sb)_2Te_3$ layers have a considerable roughness, it may be that the percolation path of the edge channel through the sample contains thinner parts which could explain an onset of this behavior in nominally thicker samples. Another explanation could be that the various capping methods (a 2-nm-thin Al layer grown *in situ* [9] or *ex situ* grown AlO_x [7]) have a different degree of effectiveness than our Te cap.

Speculation relating to the direction of magnetization in our samples.—A fine point which should be commented on relates to the direction of the magnetization vector in the sample. In the geometry examined in the theoretical literature, the magnetization is usually made to point out of the sample on all surfaces. Whether this is a necessity or how the axion physics would look for fields going inwards and outwards on opposite surfaces is not yet explored. Moreover, no direct measurement of the magnetization has yet been reported on at low enough temperatures for the samples to be in the quantized regime, where the character of the magnetization reversal is qualitatively different than that at higher temperature (See Fig. S10 in Ref. [9] for example). It is not clear if in our samples the magnetization is homogeneous, or if energy considerations (discussed in the Supplemental Material [32], which includes a reference to Ref. [35]) lead to an always inward or always outward configuration. In either event, while more investigation into this issue is certainly needed before clarity is achieved, the very fact that we observe the quantum anomalous Hall effect in the samples proves that the edge states survive, and that their scaling behavior can be analyzed.

A single species Dirac fermion on a 3D TI surface state is linked to axion electrodynamics based on gauge symmetry arguments. Scaling analysis performed on our layers is consistent with that expected from such an axion system. While uncertainty about the magnetization state leaves some degree of speculation in associating our scaling to an axion insulator, we suggest that it is a plausible explanation based on currently available evidence.

Conclusion.—We have studied the flow diagram of the QAHE in several layers. From the scaling behavior we determine that the QAHE in our capped 9-nm-thick V-doped $(Bi, Sb)_2Te_3$ layers originates from the two topological surface states of the magnetic 3D TI each contributing the half-integer quantization of $\sigma_{xy} = \frac{1}{2}e^2/h$ to the total Hall conductivity. The center of the semicircle in the flow diagram being shifted from a finite value to zero is robust evidence, which does not rely on discriminating between the various surface contributions. This result qualitatively differs from most previous publications showing 2D behavior [36] and is a robust transport observation

of a distinct QAHE having scaling properties consistent with one resulting from the presence of axionic action characterizing the electrodynamic response of a magnetic 3D TI, i.e., an axion insulator.

We gratefully acknowledge the financial support of the EU ERC-AG Program (project 3-TOP), the EU ERC-StG Program (project TOPOLECTRICS), the DFG through SFB 1170 "ToCoTronics," and the Leibniz Program.

Note added.—Recently, in addition to Ref. [36], an additional publication appeared [37] in which a 3D-like scaling (as the red dashed line of our Fig. 2) is reported in Fig. S6 of their Supplemental Material. However, as in Ref. [36], the significance of this observation was not recognized. Interestingly, in the configuration where the authors believe to have achieved a magnetization pointing out of the plane on both surfaces, the observed scaling is that of our 2D geometry (as the black dashed line of our Fig. 2), which does not support axionic response.

[1] M. Onoda and N. Nagaosa, Phys. Rev. Lett. **90**, 206601 (2003).
[2] C.-X. Liu, X.-L. Qi, X. Dai, Z. Fang, and S.-C. Zhang, Phys. Rev. Lett. **101**, 146802 (2008).
[3] R. Yu, W. Zhang, H.-J. Zhang, S.-C. Zhang, X. Dai, and Z. Fang, Science **329**, 61 (2010).
[4] Z. Qiao, S. A. Yang, W. Feng, W.-K. Tse, J. Ding, Y. Yao, J. Wang, and Q. Niu, Phys. Rev. B **82**, 161414 (2010).
[5] K. Nomura and N. Nagaosa, Phys. Rev. Lett. **106**, 166802 (2011).
[6] C.-Z. Chang *et al.*, Science **340**, 167 (2013).
[7] J. G. Checkelsky, R. Yoshimi, A. Tsukazaki, K. S. Takahashi, Y. Kozuka, J. Falson, M. Kawasaki, and Y. Tokura, Nat. Phys. **10**, 731 (2014).
[8] X. Kou, S.-T. Guo, Y. Fan, L. Pan, M. Lang, Y. Jiang, Q. Shao, T. Nie, K. Murata, J. Tang, Y. Wang, L. He, T.-K. Lee, W.-L. Lee, and K. L. Wang, Phys. Rev. Lett. **113**, 137201 (2014).
[9] A. J. Bestwick, E. J. Fox, X. Kou, L. Pan, K. L. Wang, and D. Goldhaber-Gordon, Phys. Rev. Lett. **114**, 187201 (2015).
[10] C.-Z. Chang, W. Zhao, D. Y. Kim, H. Zhang, B. A. Assaf, D. Heiman, S.-C. Zhang, C. Liu, M. H. W. Chan, and J. S. Moodera, Nat. Mater. **14**, 473 (2015).
[11] C.-Z. Chang, W. Zhao, D. Y. Kim, P. Wei, J. K. Jain, C. Liu, M. H. W. Chan, and J. S. Moodera, Phys. Rev. Lett. **115**, 057206 (2015).
[12] Y. Feng, X. Feng, Y. Ou, J. Wang, C. Liu, L. Zhang, D. Zhao, G. Jiang, S.-C. Zhang, K. He, X. Ma, Q.-K. Xue, and Y. Wang, Phys. Rev. Lett. **115**, 126801 (2015).
[13] A. Kandala, A. Richardella, S. Kempinger, C.-X. Liu, and N. Samarth, Nat. Commun. **6**, 7434 (2015).
[14] S. Grauer, S. Schreyeck, M. Winnerlein, K. Brunner, C. Gould, and L. W. Molenkamp, Phys. Rev. B **92**, 201304 (2015).
[15] X.-L. Qi, T. L. Hughes, and S.-C. Zhang, Phys. Rev. B **82**, 184516 (2010).
[16] J. Wang, B. Lian, X.-L. Qi, and S.-C. Zhang, Phys. Rev. B **92**, 081107 (2015).
[17] T. Morimoto, A. Furusaki, and N. Nagaosa, Phys. Rev. B **92**, 085113 (2015).
[18] C.-X. Liu, H. J. Zhang, B. Yan, X.-L. Qi, T. Frauenheim, X. Dai, Z. Fang, and S.-C. Zhang, Phys. Rev. B **81**, 041307 (2010).
[19] H.-Z. Lu, W.-Y. Shan, W. Yao, Q. Niu, and S.-Q. Shen, Phys. Rev. B **81**, 115407 (2010).
[20] Y. Zhang, K. He, C.-Z. Chang, C.-L. Song, L.-L. Wang, X. Chen, J.-F. Jia, Z. Fang, X. Dai, W.-Y. Shan, S.-Q. Shen, Q. Niu, X.-L. Qi, S.-C. Zhang, X.-C. Ma, and Q.-K. Xue, Nat. Phys. **6**, 584 (2010).
[21] G. Landolt, S. Schreyeck, S. V. Eremeev, B. Slomski, S. Muff, J. Osterwalder, E. V. Chulkov, C. Gould, G. Karczewski, K. Brunner, H. Buhmann, L. W. Molenkamp, and J. H. Dil, Phys. Rev. Lett. **112**, 057601 (2014).
[22] N. Tarakina, S. Schreyeck, T. Borzenko, C. Schumacher, G. Karczewski, K. Brunner, C. Gould, H. Buhmann, and L. W. Molenkamp, Cryst. Growth Des. **12**, 1913 (2012).
[23] F. Wilczek, Phys. Rev. Lett. **58**, 1799 (1987).
[24] X.-L. Qi, T. L. Hughes, and S.-C. Zhang, Phys. Rev. B **78**, 195424 (2008).
[25] L. Wu, M. Salehi, N. Koirala, J. Moon, S. Oh, and N. P. Armitage, Science **354**, 1124 (2016).
[26] V. Dziom, A. Shuvaev, A. Pimenov, G. V. Astakhov, C. Ames, K. Bendias, J. Böttcher, G. Tkachov, E. M. Hankiewicz, C. Brüne, H. Buhmann, and L. W. Molenkamp, Nat. Commun. **8**, 15197 (2017).
[27] K. Okada, Y. Takahashi, M. Mogi, R. Yoshimi, A. Tsukazaki, K. Takahashi, N. Ogawa, M. Kawasaki, and Y. Tokura, Nat. Commun. **7**, 12245 (2016).
[28] A. J. Niemi and G. W. Semenoff, Phys. Rev. Lett. **51**, 2077 (1983).
[29] A. N. Redlich, Phys. Rev. Lett. **52**, 18 (1984).
[30] M. Hilke, D. Shahar, S. H. Song, D. C. Tsui, Y. H. Xie, and M. Shayegan, Europhys. Lett. **46**, 775 (1999).
[31] M. Winnerlein *et al.* [Phys. Rev. Mater. (to be published)].
[32] See Supplemental Material at http://link.aps.org/supplemental/10.1103/PhysRevLett.118.246801 for a description of the samples, longitudinal and Hall resistances used to determine the scaling behavior, analysis of the scaling with gate voltage or temperature as the driving parameter, and the influence of layer capping, as well as a more detailed discussion on energy considerations relating to the direction of the magnetization.
[33] X. Kou, L. Pan, J. Wang, Y. Fan, E. Sang Choi, T. Nie, K. Muruta, Q. Shao, S.-C. Zhang, and K. L. Wang, Nat. Commun. **6**, 8474 (2015).
[34] K. Hilke, D. Shahar, S. H. Song, D. Tsui, Y. H. Xie, and D. Monroe, Nature (London) **395**, 675 (1998).
[35] A. S. Nunez and J. Fernandez-Rossier, Solid State Commun. **152**, 403 (2012).
[36] The external field dependence of a magnetic TI layer close to quantization shown in Fig. 1 of Kandala *et al.* [13] has a peak value of $\rho_{xx} < h/e^2$, but the implications of this behavior are neither discussed nor further investigated.
[37] M. Mogi, M. Kawamura, R. Yoshimi, A. Tsukazaki, Y. Kozuka, N. Shirakawa, K. S. Takahashi, M. Kawasaki, and Y. Tokura, Nat. Mater. **16**, 516 (2017).